Characteristic Effects of Pulsed Power Generators of Different Architecture on the Implosion Dynamics of Mid-Atomic-Number Double Planar Wire Arrays

Christopher J. Butcher, Victor L. Kantsyrev, *Member, IEEE*, Alla S. Safronova, *Member, IEEE*, Veronica V. Shlyaptseva, Austin Stafford, Paul C. Campbell, *Member, IEEE*, Stephanie M. Miller, Nicholas M. Jordan, *Senior Member, IEEE*, Ryan D. McBride, *Member, IEEE*, Adam M. Steiner, *Member, IEEE*, and Ronald M. Gilgenbach, *Life Fellow, IEEE*

***Abstract*— Planar wire arrays (PWAs) have been studied on both the University of Michigan's (UM's) low-impedance linear transformer driver (LTD), MAIZE (0.1 Ω, 0.5–1 MA, and 100–250 ns), and the University of Nevada, Reno's (UNR's) high-impedance Marx bank generator, Zebra (1.9 Ω, 1 MA, and 100 ns). Results with aluminum (low-atomic-number) and tungsten (high-atomic-number) double PWAs (DPWAs) were compared previously; thus, DPWAs made of brass (an alloy of mid-atomic-number elements copper and zinc) were recently selected for study to get a more complete understanding of low-to-high atomic number DPWA implosions on MAIZE. As the LTD is a relatively new pulsed power architecture, comparing results from traditional generators (such as Marx banks) will help us to better understand both technologies. Experimental diagnostics included an absolutely calibrated filtered polycrystalline diamond detector (PCD), filtered Si-diodes, X-ray pinhole cameras, spectrometers, and optical shadowgraphy systems. Time-dependent inductance modeling on the MAIZE LTD was derived from the measured current trace. Radiative and implosion dynamics of brass DPWAs on the MAIZE LTD are presented and compared with previous results on the Zebra Marx generator. Implosions on the MAIZE LTD featured a longer than expected current rise time that was heavily dependent upon the load inductance, as well as a longer pinching process and X-ray emission time than comparable DPWA implosions on Zebra; however, implosions on MAIZE produced L-shell plasmas comparable in characteristics with previous studies on Zebra.**

***Index Terms*— Linear transformer driver (LTD), planar wire array (PWA), plasma pinch, shadowgraphy images, X-ray spectra.**

Manuscript received 5 January 2022; revised 14 June 2022; accepted 3 August 2022. Date of publication 21 September 2022; date of current version 23 September 2022. This work was supported by the National Nuclear Security Administration (NNSA) through the Department of Energy (DOE) under Grant DE-NA0003047 and Grant DE-NA0003877 and in part by Sandia National Laboratories—a multimission laboratory managed and operated by National Technology and Engineering Solutions of Sandia, LLC, a wholly owned subsidiary of Honeywell International Inc.—the U.S. Department of Energy's National Nuclear Security Administration under Contract DE-NA0003525. The review of this article was arranged by Senior Editor S. J. Gitomer. *(Corresponding author: Christopher J. Butcher.)*

Christopher J. Butcher, Victor L. Kantsyrev, and Alla S. Safronova are with the Department of Physics, University of Nevada, Reno, NV 89557 USA (e-mail: christopherbutcher@unr.edu; victor@unr.edu; alla@physics.unr.edu).

Veronica V. Shlyaptseva was with the Department of Physics, University of Nevada, Reno, NV 89557 USA. She is now with Stratos Consulting, Boston, MA 02110 USA (e-mail: veronicashlyaptseva@gmail.com).

Austin Stafford was with the Department of Physics, University of Nevada, Reno, NV 89557 USA. He resides in Reno, NV USA (e-mail: staffo64@gmail.com).

Paul C. Campbell was with the Department of Nuclear Engineering and Radiological Sciences, University of Michigan, Ann Arbor, MI 48109 USA. He is now with the Lawrence Livermore National Laboratory, Livermore, CA 94551 USA (e-mail: pccamp@umich.edu).

Stephanie M. Miller, Nicholas M. Jordan, Ryan D. McBride, and Ronald M. Gilgenbach are with the Department of Nuclear Engineering and Radiological Sciences, University of Michigan, Ann Arbor, MI 48109 USA (e-mail: smmil@umich.edu; jordann@unich.edu; mcbrider@umich.edu; rongilg@umich.edu).

Adam M. Steiner was with the Department of Nuclear Engineering and Radiological Sciences, University of Michigan, Ann Arbor, MI 48109 USA. He is now with Sandia National Laboratories, Albuquerque, NM 87110 USA (e-mail: amsteine@umich.edu).

Color versions of one or more figures in this article are available at https://doi.org/10.1109/TPS.2022.3200574.

Digital Object Identifier 10.1109/TPS.2022.3200574

I. Introduction

LOW-IMPEDANCE linear transformer driver (LTD) architectures have been predicted to achieve greater efficiency than the traditionally used Marx-driven generators and proposed LTD machines have been designed with the potential to reach higher currents than any currently existing Marx bank machines [1], [2]. Thus, LTD architecture has been considered a potential option for future petawatt-class Z-pinch generators. The study of the radiative performance of Z-pinch generators with LTD modules is very important for the proposed prospective new LTD-based accelerators Z 300 and Z 800 at Sandia National Laboratories (SNL), Albuquerque, NM, USA [2]. The study of radiation from high-energy-density (HED) plasmas has significant applications to magnetized liner inertial fusion (MagLIF) at high-current Z-generators at SNL, as both DPWAs and MagLIF plasmas produce a central cylindrical radiating core and mid-atomic-number are used as tracers for MagLIF plasma diagnostics [3]. In contrast to larger scale machines, the availability and accessibility of university-scale pulsed power drivers make them excellent options for the development of the novel Z-pinch load configurations and are integral to progressing research on HED Z-pinch plasmas. One of the first 1-MA university-scale LTD generators was the low-impedance Michigan accelerator for inductive Z-pinch experiments (MAIZE) LTD (0.1 Ω, 0.5–1 MA, and 100–250 ns) at the University of Michigan (UM), Ann Arbor, MI, USA [4], that was used to produce results in this article.

Planar wire arrays (PWAs) have been previously shown to be excellent radiators of X-rays at the University of Nevada at Reno's (UNR's), Reno, NV, USA, high-impedance Marx bank generator, Zebra (1.9 Ω, 1 MA, and 100 ns) (see [5], [6], [7], [8], [9], [10]) as well as on the Saturn generator at SNL [11]. In particular, tungsten (W) double PWAs (DPWAs) have demonstrated the highest radiation yields amongst PWAs (up to 30 kJ), compact size (a few mm), and strong electron beams on the UNR Zebra Marx bank generator, and demonstrated applications to inertial confinement fusion research [5], [8].

Recently, low-atomic-number aluminum (Al) and high-atomic-number W DPWAs have been successfully imploded in reproducible shots on the low-impedance MAIZE LTD [12], [13], [14]. Such results could be applicable to the new compact hohlraum design with parallel-driven DPWA X-ray sources, first tested on the high-impedance Zebra generator [8], [9]. Thus, the experiments with PWAs on university-scale LTD generators (such as MAIZE) may be vitally important for the future of the inertial confinement fusion program. Also, as the LTD is a relatively new pulsed power generator architecture, it is essential to understand how Z-pinch HED plasmas perform on currently active LTD machines and make comparisons to results from similar load configurations imploded on more traditional pulsed power devices, such as Marx banks, which have been used extensively for past experiments.

However, very little information is available for mid-atomic-number wires imploded on a low-impedance LTD machine. For this reason, brass DPWAs were chosen for study on the MAIZE LTD. Brass presents a unique opportunity to study two mid-atomic-number elements, Cu and Zn, which made it a great candidate for study in conjunction with the existing data on low-atomic-number Al and high-atomic-number W DPWAs on the MAIZE LTD. In addition, previous results of brass DPWAs imploded on the high-impedance UNR Zebra Marx bank were presented in [7], where it was found that brass PWAs provided a unique opportunity to study L-shell radiation from Cu and Zn, with relatively low opacity effects in L-shell lines. The previous studies of brass DPWAs on Zebra also contributed to the decision to study brass DPWAs on MAIZE, as the comparison of implosion and radiative characteristics on both machines would further our understanding of this particular load on the MAIZE LTD.

II. Experimental Details

New experiments with brass DPWAs were carried out on the UM low-impedance MAIZE LTD and compared with earlier experiments with brass DPWAs on the UNR high-impedance Zebra Marx bank generator. MAIZE is a single-cavity, low impedance (0.1 Ω), 1-MA class LTD with 100 ns rise time into an impedance matched load, which stores 7.9 kJ in its capacitors. Zebra is a high-impedance (1.9 Ω), 1-MA (or up to 1.7 MA when the load current multiplier (LCM) is applied [15]) Marx bank generator with a 100 ns rise time, which stores 150 kJ in its capacitors. The LTD cavity design allows for multiple cavities to be connected in series to increase the generator energy. Understanding how DPWAs perform on a single-cavity, low-impedance LTD machine, as well as a high-impedance machine, is vital for understanding how DPWAs could perform on multicavity, relatively higher impedance LTD machines, such as the MYKONOS machine at Sandia National Laboratories and other prospective machines [2], [16].

The DPWAs consisted of two wire planes of micrometer-scale diameter brass wires [see Fig. 1(c)]. The DPWA masses were calculated from the number of wires, the diameter of the wires, and the wire material. In [6], it was observed that DPWA implosion dynamics depend strongly upon the aspect ratio ϕ, defined as the ratio of the array width to the interplanar gap. In the following sections, we present results from two brass DPWAs of different aspect ratios (a lower aspect ratio $\phi = 1.67$ and a higher aspect ratio $\phi = 2.33$) imploded on the MAIZE LTD generator (see Fig. 1 and Table I). The anode–cathode gap was 1 cm, while the interwire gap was 1 mm.

Due to the relatively large inductance of the DPWA load hardware, the MAIZE LTD was limited to 70% of the maximum charge voltage to prevent damage to the main (central) insulator and minimize voltage reversal on the capacitors. Under these operating conditions, the peak current was roughly 500 kA and the rise time ranged from 180 to 210 ns.

The DPWA experiments on MAIZE largely shared the same diagnostics that were used on the UNR Zebra Marx bank generator (see Figure 1). On the MAIZE LTD [Fig. 1(a)], the load is housed in the center of a circular, 1-m-diameter vacuum chamber located in the center of the 3-m-diameter cavity. Experimental diagnostics were located inside and outside the vacuum chamber. Diagnostics included various filtered X-ray diodes; X-ray spectrometers and X-ray pinhole cameras; a filtered Faraday cup placed above the load for measurement of the electron beam; an ultrafast, intensified, 12-frame camera for use in shadowgraphy/self-emission imaging (while only shadowgraphy is presented in this article, self-emission imaging was presented in [14]); and B-dot loops at four azimuthal locations on the radial transmission line for measurement of the time-resolved current pulse. Results of electron beam measurements made with the Faraday cup above the anode will be the subject of a future publication.

A side-on absolutely calibrated filtered polycrystalline diamond detector (PCD) with a time resolution of 0.5 ns was used to record X-ray emission throughout the pinching process. The PCD was filtered to detect photons with energies above the cutoff energy of 2.4 keV. For the purposes of this work, the cutoff energy E is defined as the energy where the transmission through the filter drops to a value of $1/e$, where e is the base of the natural logarithm. In addition to the PCD, three side-on, cross-calibrated AXUV-HS5 Si-diodes (SiDs) with a time resolution of 1 ns were implemented to measure time-resolved X-ray output in three energy bands: >1.4, >3.5, and >9 keV. All diode detectors were placed such that the lines of sight aligned within 15° with respect to the planes of the arrays [i.e., the line of sight that looks into the gap between the planes, see Fig. 1(d)]. The oscilloscopes used featured a 500-MHz bandwidth and 5-GS/s sample rate, capable of resolving the PCD time resolution.

Two side-on time-integrated X-ray spectrometers were applied to measure electron temperature (T_e), electron density (N_e), and opacity effects of the brass Z-pinch plasmas, using

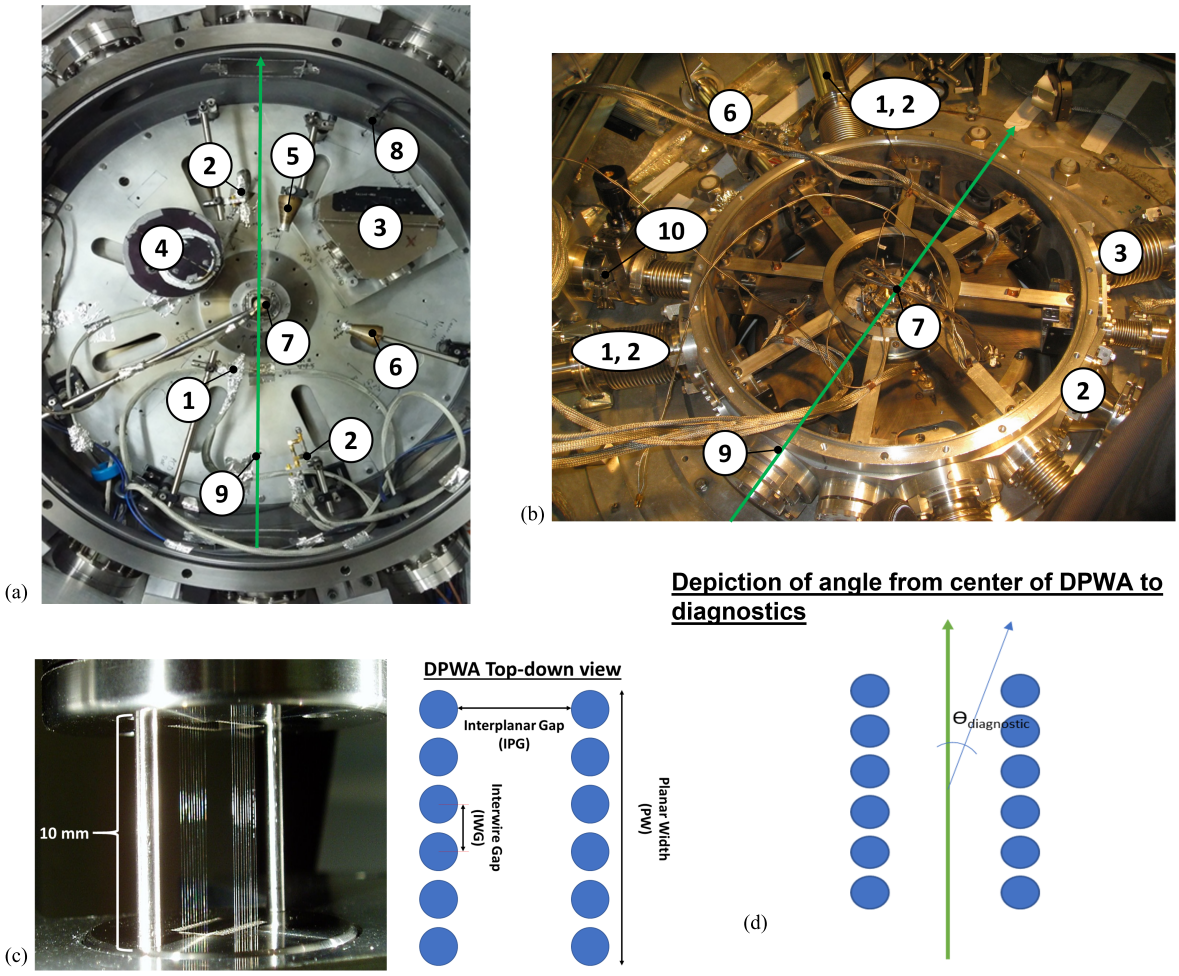

Fig. 1. (Color online). (a) Top-down image of the MAIZE LTD vacuum chamber, with X-ray and electron beam diagnostics surrounding the DPWA load in the center of the chamber: (1) X-ray PCD; (2) SiD; (3) soft X-ray KAP-crystal spectrometer; (4) hard X-ray LiF-crystal spectrometer; (5) X-ray pinhole camera placed along the load wire planes; (6) X-ray pinhole camera placed orthogonal to the wire planes; (7) Faraday cup detector placed above the load in the center of the chamber; (8) B-dot sensors placed along the edges of the chamber 90° from each other (not all B-dot sensors are visible in this image); and (9) green arrow representing the optical probing beam path/camera line of sight through the chamber and load. (b) Top-down image of the Zebra Marx bank vacuum chamber, with X-ray and electron beam diagnostics surrounding the DPWA load in the center of the chamber. Many of the same diagnostics were shared between MAIZE and Zebra (diagnostic numbers are the same). (c) Image and top-down diagram of a DPWA load. The interplanar gap and planar width are shown to highlight the determining factors of the DPWA aspect ratio. (d) Diagram of the angle from the center of the DPWA to the respective diagnostics. The green arrow represents the center line of the load, looking down between the planes of the DPWA (the same line of sight as the shadowgraphy laser), while the blue arrow represents the direction of the diagnostic. The angles to all diagnostics are measured from the center (i.e., angles range from 0°–90°).

TABLE I

EXPERIMENTAL PARAMETERS TESTED ON MAIZE. THE IMPLOSION TIMES ARE MEASURED RELATIVE TO THE START OF THE CURRENT PULSE. THE RADIATED ENERGIES ARE FOR THE >2.4 keV BAND, INTEGRATED OVER THE DURATION OF THE EXPERIMENT. THE ERROR IN ENERGY CALCULATIONS WAS 35% [13]. ASYNCHRONOUS LTD SWITCH FIRING TIMES AND CURRENT LOSS IN THE MITL REGION ARE FACTORED INTO AN ESTIMATED ERROR OF APPROXIMATELY 50 kA IN THE MAXIMUM CURRENTS LISTED

MAIZE Shot	Material	Load	Aspect Ratio	Mass (μg/cm)	Current Max (kA)	Current Risetime (ns)	Implosion Time (ns)	Energy over 4π (J)
1249	Brass	DPWA	1.67	57	462	180	224	0.53
1250	Brass	DPWA	2.33	76	475	210	230	0.77

nonlocal thermal equilibrium (non-LTE) kinetic models [7], [17], [18]. The two spectrometers were employed to measure X-rays in two different X-ray bands: a softer X-ray spectral region between 4 and 13 Å and a harder region between 1 and 2.4 Å. The softer X-ray spectrometer had a convex potassium acid phthalate (KAP) crystal with a double lattice spacing

$2d = 26.63$ Å, a radius of curvature of 51 mm, a 1-D axial spatial resolution of 4 mm, and a spectral resolution $R = \lambda/\Delta\lambda = 500$. The harder X-ray spectrometer had a convex lithium fluoride (LiF) crystal with a double lattice spacing $2d = 4.027$ Å, a radius of curvature of 25.4 mm, and a 1-D axial spatial resolution of 4 mm. The spectrometers were equipped with 7.5-μm-thick Kapton film together withk 3-μm-thick Mylar (aluminized on both sides with 0.15-μm-thick Al layers) to protect the film from unwanted outside light. The spectra themselves were recorded onto Kodak Biomax MS X-ray film, with grain size 0.12 ± 0.03 μm [19], [20].

The non-LTE kinetic models for Cu and Zn were originally developed to analyze spectra from the Zebra generator [7], [17], [18]. The Cu and Zn models include the ground states as well as singly and doubly excited states, and atomic details for H- to Al-like ions. The atomic data is calculated using the flexible atomic code (FAC) [21]. Given plasma parameters (T_e and N_e), the Cu and Zn kinetic models generate synthetic spectra. The synthetic spectra of L-shell Cu and Zn were then compared with the experimentally measured spectra, and the plasma parameters of best fit are chosen to determine the experimental plasma parameters. The primary factor in determining the electron density was the relative intensities of the Ne-like 3F or 3G lines compared with the Ne-like 4C line, while the electron temperature was inferred by comparing the relative intensities of neighboring ionization stages. The uncertainty of T_e estimates is about 10%, while N_e is about 20%–30% [7].

The two side-on X-ray pinhole cameras (spatial resolution of 90 μm) were placed approximately 90° apart from each other to view the load from both the "front" and "side" views; the first was placed within 15° or less, with respect to the planes of the arrays, while the second was placed at approximately $80° \pm 5°$ [see Fig. 1(d)]. Each pinhole can record three independent, time-integrated X-ray images (filtered to detect >1.4, >1.6, and >3.5 keV X-rays) using the same X-ray film.

An intensified, ultrafast, 12-frame camera was used in conjunction with a 532-nm, 2-ns, frequency-doubled Nd:YAG pulse, split into optical beams with a 10-ns delay between each beam, for use as a backlighting source for shadowgraphy images [22]. Images were taken prior to and throughout the Z-pinching process to study the plasma evolution. All imaging windows for MAIZE shots presented in this article began prior to the main pinch, with 10-ns exposure per frame, to include images of early standing shock and precursor plasma column development.

Four B-dot probes, radially located approximately 0.4 m from the load at the center of the chamber and equally spaced azimuthally (90° between adjacent probes) were used to measure the time-resolved current trace throughout the Z-pinch. As the MAIZE LTD is a low-impedance machine, the change in inductance of the plasma load throughout the Z-pinching process has a larger effect on the current trace compared to stiffer (high-impedance) drivers like the UNR Zebra Marx generator. The effect that the load inductance has on the current trace can be explored by comparing the measured current trace to a simulated, static inductance (nonimploding) load to calculate an effective inductance of the load throughout the Z-pinch as a function of time. This method is explained in detail in [14] and [23].

The wire ablation dynamics model (WADM) simulates the implosion dynamics and wire ablation through the approximation of the wire material as discrete thin filaments with mass, velocity, and the capability to conduct current [6], [7], [24], [25], [26]. The model works by first inputting the generator and load parameters. The load parameters include the thickness of the wires, the total wire mass, the interplanar and interwire gap spacing, and the ablation rate coefficient, which is an intrinsic property of the wire material [25], [26]. The model then calculates the inductive current distribution between the wires and the magnetic field contribution for each individual wire throughout the duration of the pinch. Each wire is taken to be an individual filament, where the model simulates ablated coronal plasma with kinetic energy and acceleration of each filament determined by the calculated magnetic field. For this work, the WADM model was used to calculate the location of material mass accumulation throughout the pinching process, and comparisons to shadowgraphy imaging.

Experiments on Zebra featured similar load parameters, and are largely discussed in [7]. As mentioned earlier, many of the same diagnostics used on MAIZE were also implemented on Zebra. In addition, experiments on Zebra featured a time-gated KAP spectrometer and a time-gated pinhole camera. The UNR Zebra Marx bank itself also differs greatly from the UM MAIZE LTD. The brass DPWAs imploded on Zebra were both 8/8 wire arrays (meaning each plane was made up of eight wires), with a lower aspect ratio of $\phi = 1.63$, 124-μg mass, and a 2-cm anode–cathode gap. As Zebra is a high-impedance and high-energy generator, the array masses on Zebra can be higher than on MAIZE (the array masses presented in [7] on Zebra were $2\times$ heavier than those presented in this work on MAIZE); however, the lower aspect ratio brass DPWA on MAIZE was chosen to achieve a similar aspect ratio to the previously presented brass DPWAs on Zebra ($\phi = 1.67$ on MAIZE and $\phi = 1.63$ on Zebra).

III. Implosion and Radiative Properties of Brass DPWAs on the Zebra Marx Bank Generator for Comparison With Present MAIZE Results

In [7], the radiative characteristics and implosion dynamics of two brass DPWAs (Zebra Shot# 1036 and Zebra Shot# 1257) were presented. Both brass DPWAs had identical array configurations (8/8 wire arrays, aspect ratio $\phi = 1.63$, and 124-μg array mass). The brass DPWA Zebra Shot# 1036 (see [7, Fig. 5]) was successfully imploded on the Zebra Marx bank, though it had an uncharacteristically long current rise time for Zebra, of approximately 170 ns. The X-ray burst began around 170 ns, approximately the same as the rise time, and lasted until 220 ns, making for a total emission time of roughly 50 ns, as measured by the PCD, which, in that work, was only measured once and was filtered at >0.75 keV [7]. The time-gated spectroscopic analysis showed a good correlation with the X-ray burst, with the plasma reaching a maximum electron temperature T_e of 450 eV in

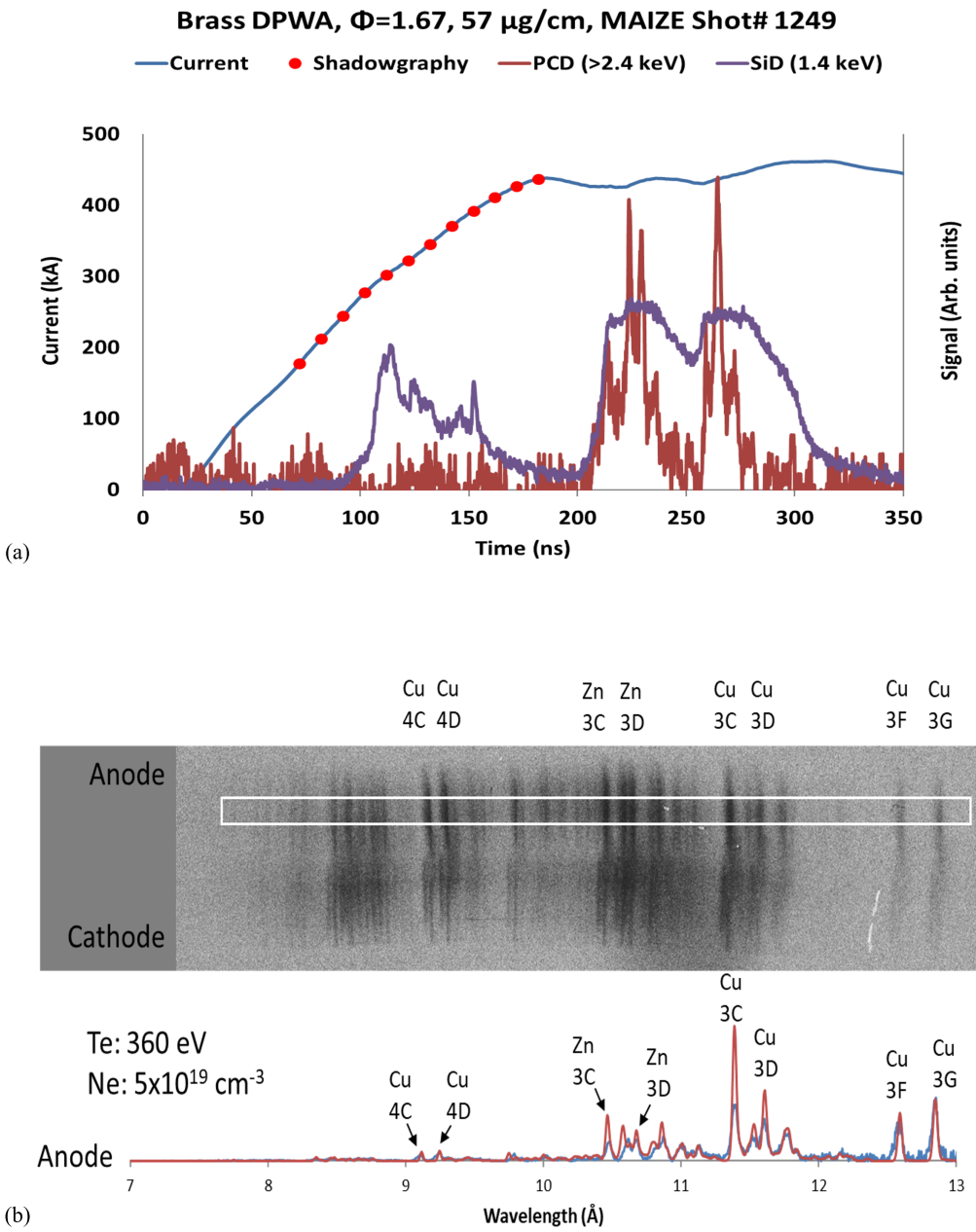

Fig. 2. (Color online). Brass DPWA, $\phi = 1.67$, MAIZE Shot# 1249 (6/6, interplanar gap = 3 mm, interwire gap = 1 mm, and array mass = 57 μg/cm). (a) PCD signal (dark red) shows radiation in the >2.4 keV region, while the SiD signal (purple) shows the radiation signal in >1.4 keV spectral band. Current (blue) rise time was 180 ns with main implosions occurring at 200–240 ns and at 255–280 ns from the start of current. Red dots correspond to moments when a shadowgraphy image was taken (see Fig. 3). (b) One-dimensional spatially resolved, time-integrated X-ray spectrum is compared with theoretical modeling to find plasma conditions of $T_e = 360$ eV and $N_e = 5 \times 10^{19}$ cm^{-3} near the anode.

time with the peak of X-ray radiation burst, and an electron density N_e on the order of 10^{19} cm^{-3}. Zebra Shot# 1257 also imploded successfully, and featured a similar current rise time and radiation burst timing to Zebra Shot# 1036 (see [7, Fig. 8]), as measured by the PCD. The spatially resolved, time-integrated spectra from Zebra Shot# 1257 showed an electron temperature of 450 eV near the anode and 400 eV near the cathode. In addition to the good correlation with the X-ray signal, analysis of the time-gated spectra showed a good correlation with maximum values from the time-integrated spatially resolved spectra, being the hottest at the peak of X-ray emission. The non-LTE spectral modeling for brass DPWAs showed evidence of strong opacity effects in the most intense L-shell Cu and Zn lines, notably the Ne-like lines: Cu 3C, Cu 3D, and Zn 3C [7].

IV. Radiative Properties of Brass Double Planar Wire Arrays on the MAIZE LTD

Multiple brass DPWAs of different configurations were successfully imploded on the MAIZE LTD generator. The shots analyzed in this article represent two different aspect ratios ($\phi = 1.67$ and 2.33) and featured relatively high X-ray output. MAIZE Shot# 1249, shown in Fig. 2, was chosen to

display the results of the lower aspect ratio, $\phi = 1.67$, and MAIZE Shot# 1250, shown in Fig. 4, was chosen to display the results of the higher aspect ratio, $\phi = 2.33$, and brass DPWAs.

A. MAIZE Shot# 1249, Brass DPWA, $\phi = 1.67$, Radiative Properties

As can be seen in Fig. 2(a), the lower aspect ratio, $\phi = 1.67$, brass DPWA MAIZE Shot# 1249 (6/6, interplanar gap = 3 mm, interwire gap = 1 mm, and array mass = 57 μg/cm), featured a current rise time of 180 ns, with the initial implosion and radiation burst beginning around 200 ns, which corresponds to a dip in the current trace. This dip in current is attributed to a drastic change in load inductance during the pinch, which will be discussed further in Section V. The implosion featured two distinct radiation bursts, which were detected by both the SiD measuring in the >1.4 keV band, as well as the PCD, measuring in the >2.4 keV band. The first burst reached its peak at 225 ns after the start of the current with the second burst reaching its peak at 265 ns. The first burst began radiating around 200 ns and finished at 250 ns, while the second began radiating soon after at 255 ns and radiated up to 275 ns, making for a total X-ray emission time of approximately 75 ns in the >2.4 keV band for the main pinch. It should be noted that both bursts reached relatively the same peak maximum. The >1.4 keV band also featured two distinct peaks, but radiated longer, the second burst radiating until approximately 300 ns, making for a total emission time of approximately 100 ns in the >1.4 keV band. The load also began radiating in the >1.4 keV band earlier than the main pinch, beginning at approximately 80 ns and radiating up to 180 ns.

The spatially resolved time-integrated X-ray L-shell spectra of Cu and Zn were analyzed using the S-UNR code, a non-LTE code developed at UNR [7], [17]. The spectral analysis from MAIZE Shot# 1249 [Fig. 2(b)] revealed an electron temperature (T_e) of 360 eV and density (N_e) of 5×10^{19} cm^{-3} near the anode and demonstrates the evidence of optically thick Cu 3C and Zn 3C Ne-like lines.

Fig. 3 shows the shadowgraphy images taken throughout the implosion of MAIZE Shot# 1249, from 72 to 182 ns after the start of the current, alongside WADM simulations of the same time. From these images, it can be seen that mass accumulation along the central axis formed a central "precursor" column (the precursor column is the accumulation of early ablated mass that gathers along the central axis prior to the pinch), beginning around 82–92 ns after the start of current. However, it can also be observed that the other precursor column "bent" toward one side of the load. The cause of this asymmetrical earlier formation is not yet fully understood. It can also be observed that there is a noticeable rise in the brightness of the central precursor column, beginning at 102 ns, as the central column began to draw some current away from the planes. This can be perceived in the shadowgraphy images as the background (the brighter areas not consisting of the ablating wires and central column) becomes noticeably darker, as the radiating column becomes a source of light, impeding the laser light source. This also corresponds to the beginning of the earliest (and lowest magnitude) radiation burst in the >1.4 keV band [see Fig. 2(a)]. Standing shocks can also be observed, forming around the 102-ns mark (see [6] for a detailed explanation of standing shocks and how they form). WADM modeling showed a good correlation with the shadowgraphy images as well, i.e., mass accumulation along the central axis beginning around 82 ns and drastically increasing around 102–112 ns. Likewise, the WADM simulation shows an increase in mass accumulation around the central precursor column beginning around 102–112 ns, correlating to the formation of the standing shocks. The mass accumulation along the central axis beginning to draw current from the outer ablating wires into the central axis causes a noticeable "dip" in the current trace (though not as drastic as the main pinches), which corresponds to a rise in the load inductance (see Section V).

B. MAIZE Shot# 1250, Brass DPWA, $\phi = 2.33$, Radiative Properties

The X-ray diode signals and current trace for the higher aspect ratio Shot# 1250 (8/8, interplanar gap = 3 mm, interwire gap = 1 mm, and array mass = 76 μg/cm), are shown in Fig. 4(a). Similar to the lower aspect ratio load, the higher aspect ratio load featured two distinct radiation bursts which were detected in both the >1.4 keV band by a filtered SiD and the >2.4 keV band, detected by the PCD. However, the first X-ray burst in the >2.4 keV region reached a much higher relative peak than the second, later burst in the >2.4 keV band. The current rise time was slower than on the lower aspect ratio, with the current reaching its peak at 210 ns after the start of the current. The first X-ray burst in the >2.4 keV region followed soon after, beginning at approximately 220 ns and radiating up to 245 ns. The second burst in the >2.4 keV band began radiating much later, at about 280 ns, and continued radiating up to 300 ns. Unlike in the lower aspect ratio load, the first burst was much more intense than the secondary burst, reaching a much higher relative maximum peak. This is likely due to the additional mass imploded, as Shot# 1250 was more massive than Shot# 1249. There was a large break between the two distinct peaks, from 245 to 280 ns, in which the load was not radiating, or radiating very little, in the >2.4 keV band. However, the load continued to radiate in the >1.4 keV band consistently from 225 ns to 315 ns, reaching relative peaks at 235 ns and 285 ns, which corresponded to the relative maximum peaks in the >2.4 keV band as well.

The non-LTE modeling of L-shell spectra of Cu and Zn from MAIZE Shot# 1250 [Fig. 4(b)] revealed an electron temperature of 360 eV and density of 5×10^{19} cm^{-3}, and the evidence of optically thick Cu 3C and Zn 3C Ne-like lines near the anode, with similar parameters ($T_e = 350$ eV and $N_e = 3 \times 10^{19}$ cm^{-3}) and a less optically thick Cu 3C line near the cathode. The comparisons with the Zebra results from [7] will be given in Section VI.

We see a small burst early in time, from 75 to 150 ns from the start of the current. Once again, this less intense, early X-ray burst in the >1.4 keV band corresponds to the formation of the precursor column (see Fig. 5). Again, once the precursor

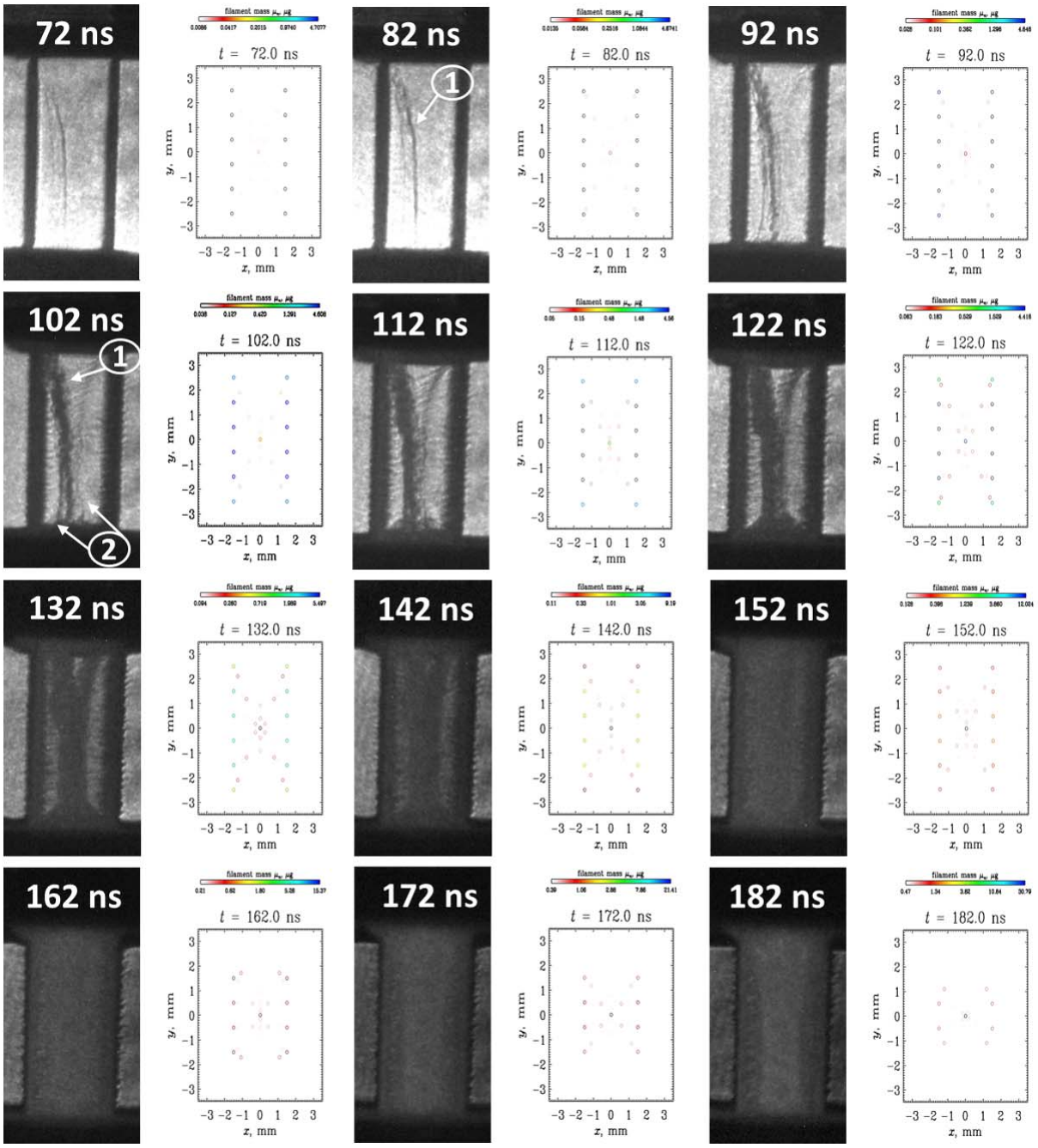

Fig. 3. Side-by-side comparison of shadowgraphy images and WADM modeling from MAIZE Shot# 1249 show the implosion evolution in time from the start of current. The central precursor column is highlighted with a ①, while the standing shocks are labeled with a ②. Note the drop in background brightness at the 102-ns mark.

column has accumulated enough mass, a portion of the current begins to flow through the column, resulting in low levels of radiation. It can also be observed that standing shocks form around the 74-ns point; however, these seem to have dissolved by the 104–114-ns point. This is an interesting phenomenon, as these standing shocks have not been observed in DPWAs of this high aspect ratio on the Zebra generator, as the wide array width makes it difficult for the global magnetic field to penetrate into the interior of the array, causing the mass to accumulate along the saddle points [6]. While the shocks are short-lasting, their formation indicates that the global magnetic field was able to penetrate the interior of the load during the current rise. This is likely due to the lower current and energy of the MAIZE machine, as the current going through each plane created magnetic fields that operated, somewhat, independently of each other. Once the current was suitably high, however, this seemed to have dissolved the standing shocks as the magnetic fields from each plane were joined into one global magnetic field. This has likely not been observed on the Zebra generator for this high value of aspect ratio, as the high current and energy of the Zebra generator do not allow for this to occur on higher aspect ratio loads, as it does for

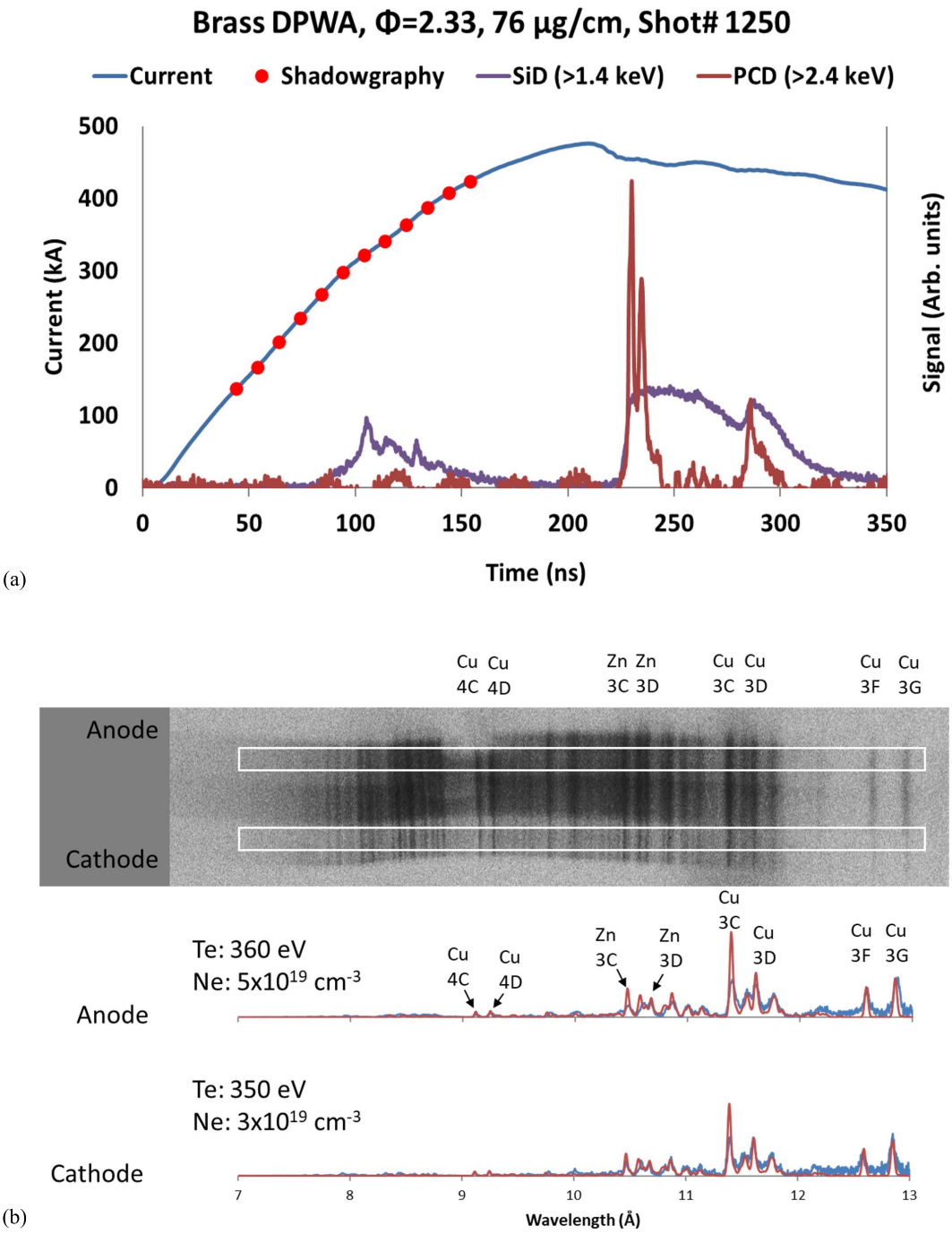

Fig. 4. (Color online). Brass DPWA, $\phi = 2.33$, MAIZE Shot# 1250 (8/8, interplanar gap = 3 mm, interwire gap = 1 mm, and array mass = 76 μg/cm). (a) PCD signal (dark red) shows radiation in the >2.4 keV region, while the SiD signal (purple) shows the radiation signal in >1.4 keV spectral band. Current (blue) rise time was 200 ns with the main implosion occurring at 220–245 ns and a smaller, secondary implosion occurring at 280–300 ns from the start of current. Red dots correspond to moments when a shadowgraphy image was taken. (b) One-dimensional spatially resolved, time-integrated X-ray spectra are compared with theoretical modeling to find plasma conditions of $T_e = 360$ eV and $N_e = 5 \times 10^{19}$ cm^{-3} near the anode and $T_e = 350$ eV and $N_e = 3 \times 10^{19}$ cm^{-3} near the cathode.

low- and mid-range aspect ratios. The WADM modeling showed a good correlation with the formation of the precursor column, as it demonstrates an increase in the mass accumulation along the central axis beginning around the 74-ns point (see Fig. 5).

C. Total Radiated Energy Output Analysis

The X-ray yields of the imploded DPWAs were approximated by integrating the signals from the absolutely calibrated PCD over the entire duration of emission and assuming isotropic radiation into 4π steradians. The anisotropy of total X-rays for DPWAs was previously found to be small (~10%–20%) for similar DPWA configurations [27]. The total X-ray yield in >2.4 keV region for the lower aspect ratio (MAIZE Shot# 1249 and $\phi = 1.67$) brass DPWA was measured to be ~0.53 J, while for the higher aspect ratio (MAIZE Shot# 1250 and $\phi = 2.33$) it was measured to be ~0.77 J (see Table I).

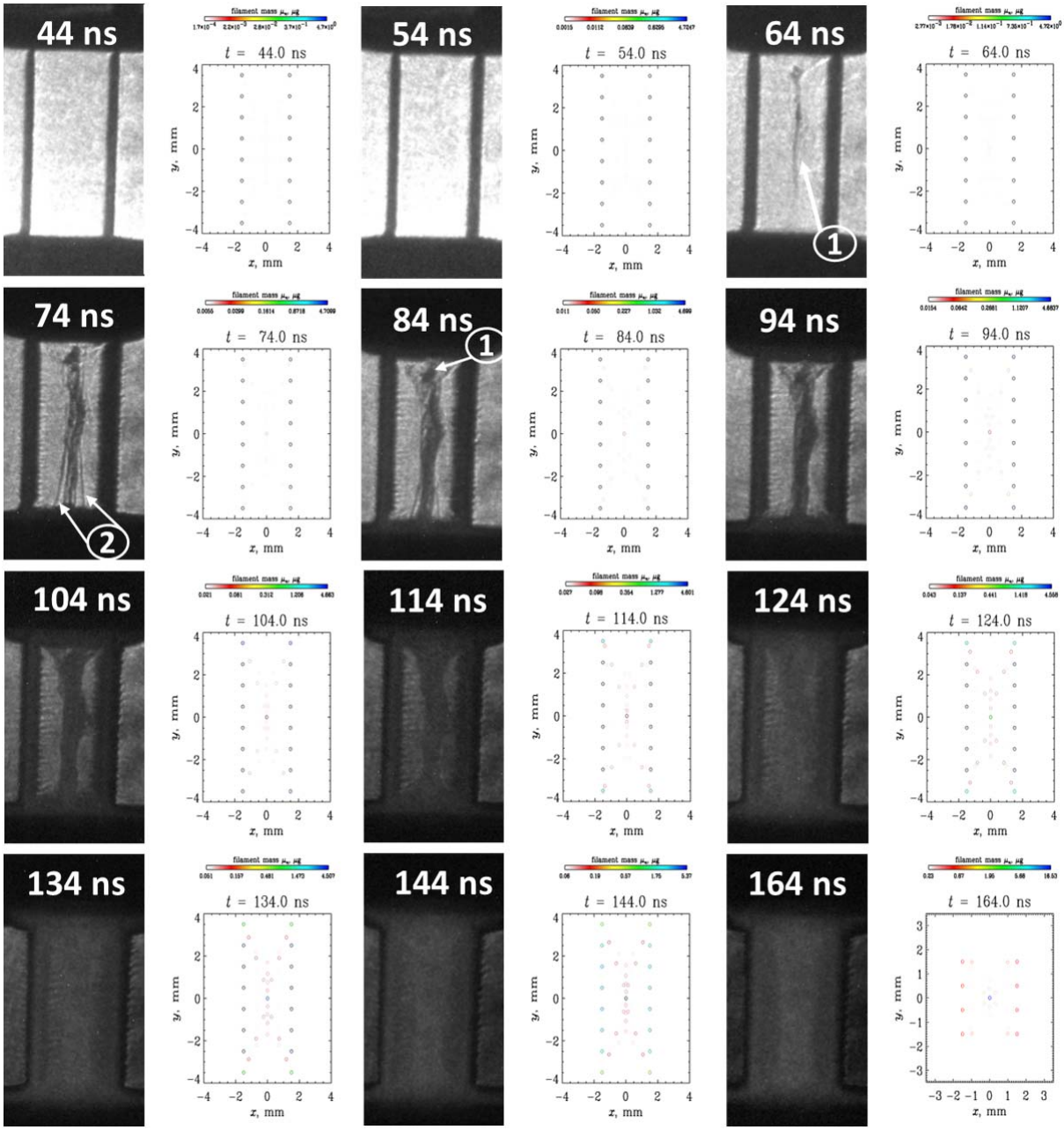

Fig. 5. Side-by-side shadowgraphy images and WADM simulations from MAIZE Shot# 1250 show the implosion evolution in time from the start of current. The central precursor column is highlighted with a ①, while the standing shocks are labeled with a ②. Note the drop in background brightness at the 74-ns mark.

Recent data from [14] presented implosions of high-atomic-number W and low-atomic-number Al DPWAs on the MAIZE LTD. The data on Al and W DPWAs was chosen to represent similarly low- to mid-ranging aspect ratio DPWAs (ϕ = 0.58 for Al and ϕ = 1.05 for W) to MAIZE Shot# 1249. In [14], the W DPWA was found to be the highest radiator of X-rays in the >2.4 keV band, with an estimated total output of 1.6 J, while the Al DPWA was found to be the lowest radiator (amongst DPWAs) with a total >2.4 keV X-ray output energy of 0.067 J. By comparing the X-ray outputs in [14] with the data from brass DPWAs in this work, it was found that the total radiated energy in the >2.4 keV band increases with atomic number. Low-atomic-number Al produced the lowest yield, mid-atomic-number brass produced the next highest, and high-atomic-number W produced the highest yield.

V. Inductance Modeling of Brass DPWAs on the UM MAIZE LTD Generator

As the UM MAIZE LTD generator is a low-impedance machine (0.1 Ω), the changes in partial self-inductance of the imploding region of the load (the wire array) throughout the pinching process can drastically affect the current trace. A better understanding of how the pinching process affects the current will help to better optimize future loads on the UM MAIZE LTD, as well as other low-impedance pulsed power drivers, both existing and future. The dependence of

the current trace on the load inductance can be exploited to allow us to extract information about the time evolution of the inductance of a load from a measurement of current. This is done by simulating a current pulse through a static load of equal inductance to the load, once the load has entered the plasma phase, but prior to implosion, and then comparing that with the measured current trace. The time at which the load enters the plasma phase can be seen on the measured current trace as a "notch" in which the slope of the measured current trace lowers, around 50–60 ns after the start of the current. This method is discussed in detail in [23] and was revised in [14] to better account for the loss in power associated with the mechanical energy driving the load implosion. The calculations in this article use the revised methods described in [14], in which the initial inductance calculation is iterated until the difference between the preceding and proceeding iterations falls within a designated convergence criterion (in this work, the convergence criterion was 0.1 nH).

Using the calculated initial load inductance and characteristic resistance, a simulated current is calculated in which the pinch does not occur and the load is static. Originally, the time-dependent inductance was calculated by finding the difference in the simulated and measured traces, and computing

$$L(t) = L(0)\frac{I_{\text{sim}}^2}{I_{\text{meas}}^2} \tag{1}$$

where L(t) is the *effective* time-dependent inductance associated with the total driver-load circuit, $L(0)$ is the initial inductance of the circuit prior to the start of current, I_{sim} is the simulated current pulse, and I_{meas} is the measured current pulse [13], [23]. This method was later revised in [14] to account for the power associated with the mechanical energy driving the load implosion [28]. A modified calculation was then implemented to solve for the inductance iteratively, to account for this energy-transfer mechanism. In this method, the initial guess for $L(t)$ is calculated in the previous manner, but the notation is changed to allow for future iterations; so $L(t)$ then becomes

$$L(t) = \frac{L_0 I_{\text{sim\_0}}^2}{I_{\text{meas}}^2} = \frac{2E_0}{I_{\text{meas}}^2} \tag{2}$$

where E_0 is the energy stored in the magnetic field. Then, we calculate the implied change in the electromagnetic energy stored in the cavity as a function of time

$$\Delta E(t) = -\frac{1}{2}\int \frac{dL_i}{dt} I_{\text{meas}}^2 dt \tag{3}$$

and L is then recalculated by

$$L_{i+1}(t) = \frac{2(E_0 + \Delta E(t))}{I_{\text{meas}}^2} \tag{4}$$

to get the next iteration. The inductance is then calculated by comparing $L_{i+1}(t)$ and L_i(t), finding the maximum error over the interval of interest, and continuing to iterate with (3) and (4) until the error falls below the specified convergence criterion (0.1 nH).

A. MAIZE Shot# 1249, Brass DPWA, $\phi = 1.67$, Time-Resolved Inductance Modeling

As is shown in Fig. 6, the relative maxima in the inductance showed a good correlation with the timing of X-ray bursts. The inductance begins to rise sharply around 90 ns after the start of the current, coinciding with the formation of the standing shocks. The first relative maxima of 4 nH are reached at approximately 125 ns after the start of the current, which corresponds well to the first, less intense X-ray burst in the >1.4 keV band, and the formation of the precursor column. Similar to the X-ray bursts, the inductance also reached two relative maxima at 220 and 255 ns. The first inductance peak of the main bursts, occurring at 225 ns, reached an overall maximum of 8.9 nH, while the second inductance peak reached a relative maximum of 8.7 nH at 255 ns. Typically, the peak inductance correlates with the strength of the pinch, which coincides with the intensity of the X-ray burst, as the inductance is directly correlated with the effective current carrying radius. A smaller pinch radius typically correlates to a hotter and denser plasma and a higher X-ray output. It should be noted that, while both peaks of the main X-ray bursts reached approximately the same peak amplitude, the first X-ray burst (occurring at 225 ns) had a much longer duration of X-ray emission than the proceeding, final burst, making for a higher overall X-ray flux, thus it makes sense that the overall maximum inductance peak occurred simultaneously with the first peak of the main X-ray burst at 225 ns.

B. MAIZE Shot# 1250, Brass DPWA, $\phi = 2.33$, Time-Resolved Inductance Modeling

From Fig. 7, we can see that the higher aspect ratio, $\phi = 2.33$, brass DPWA MAIZE Shot# 1250 followed a similar inductance time-development as the lower aspect ratio, $\phi = 1.67$, and MAIZE Shot# 1249. In MAIZE Shot# 1250, the inductance began rising sharply at 90 ns, around the time when the precursor column began to form. The inductance reached its first relative maximum of 5.3 nH at 125 ns, around the time when the precursor column fully formed. The inductance then lowered and remained nearly constant before rising again for the main pinch. During the first X-ray burst of the main pinch, at approximately 230 ns, the inductance reached a short-lived relative maximum of 7.5 nH at 230 ns, before quickly rising to its overall maximum of 7.8 nH at 245 ns, which correlated well in time to the main X-ray burst. The inductance then decreased before reaching its final relative maximum of 6.6 nH at 280 ns, coinciding with the final, less intense X-ray burst. It is interesting that the lower aspect ratio MAIZE Shot #1249 reached a higher maximum inductance of 8.9 nH, almost 1 nH higher, than the maximum reached by the higher aspect ratio MAIZE Shot #1250, despite the X-ray burst being of lower intensity than the main x-ray burst of MAIZE Shot #1250. While this phenomenon is not fully understood, it could have been caused by a nonuniform plasma column in Shot #1249, where a region of the plasma column may have reached a smaller radius, causing a spike in the inductance, while Shot #1250 may have had a more

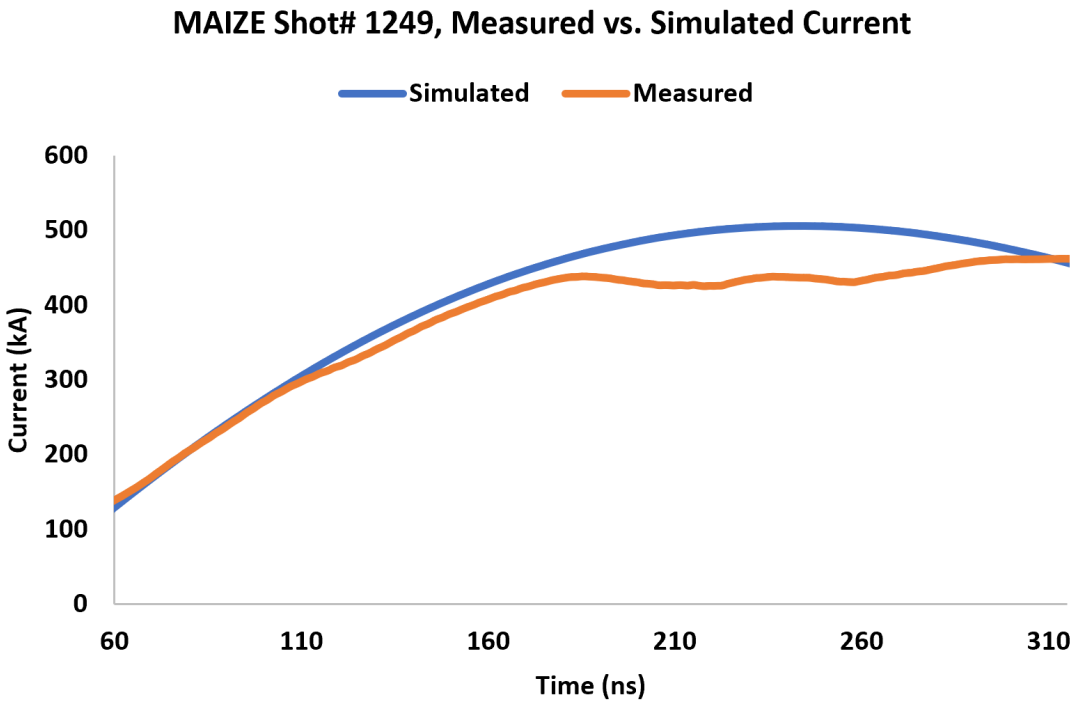

(a)

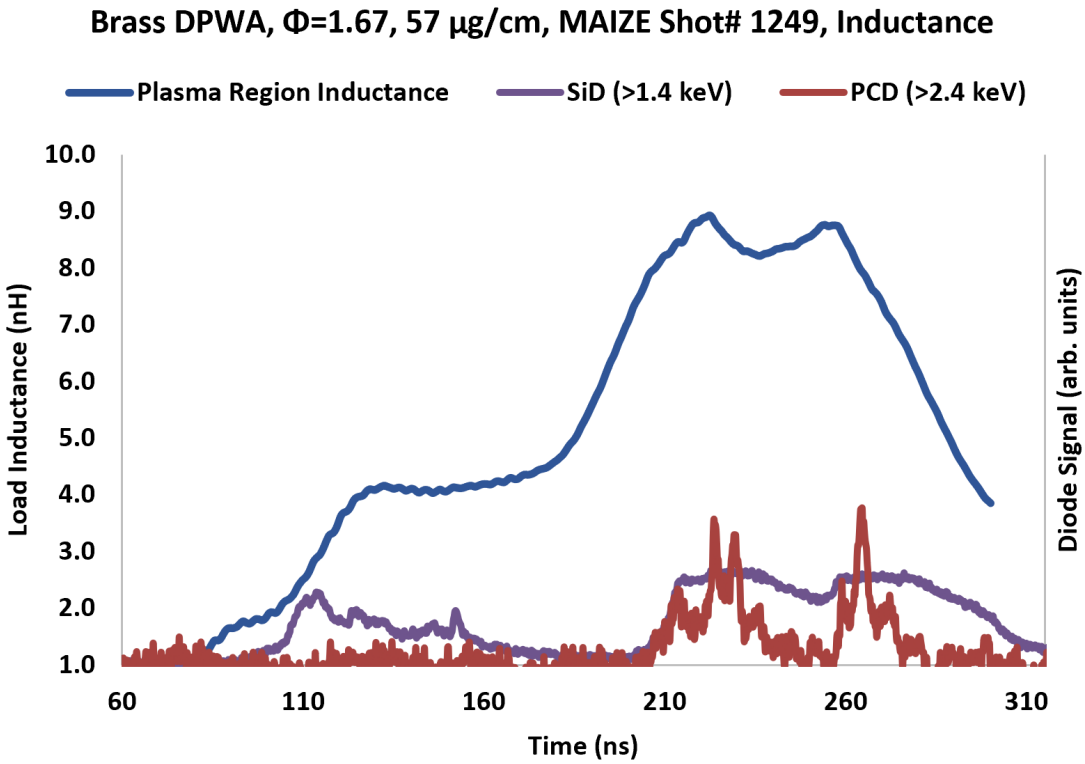

(b)

Fig. 6. (Color online). Inductance calculations from brass DPWA MAIZE Shot 1249. (a) Comparison of simulated current (blue) to the experimentally measured current (orange). (b) Time-dependent load plasma region inductance throughout the implosion (dark blue), plotted with >1.4 keV (purple) and >2.4 keV (dark red) X-ray signals.

uniform radius throughout the pinch, causing it to be more emissive of >2.4 keV radiation, but not to reach as high of an average inductance. While unconfirmed, the theory of an asymmetric pinching column during the implosion for MAIZE Shot # 1249 could have been caused by the early development of one plane beginning to implode sooner than the other

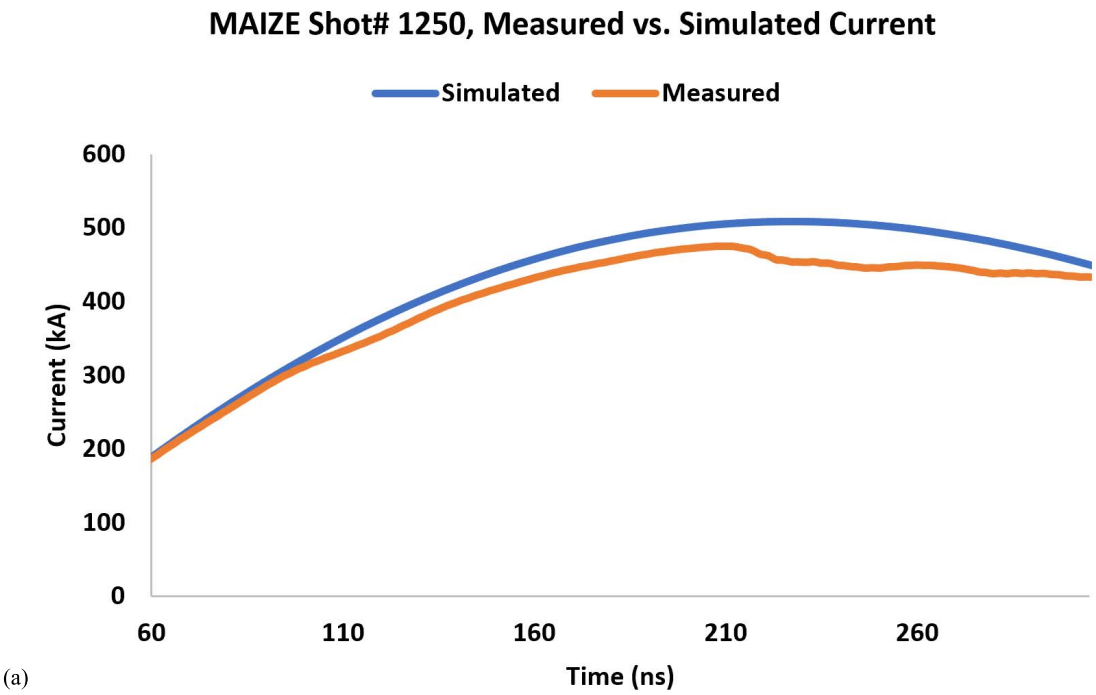

(a)

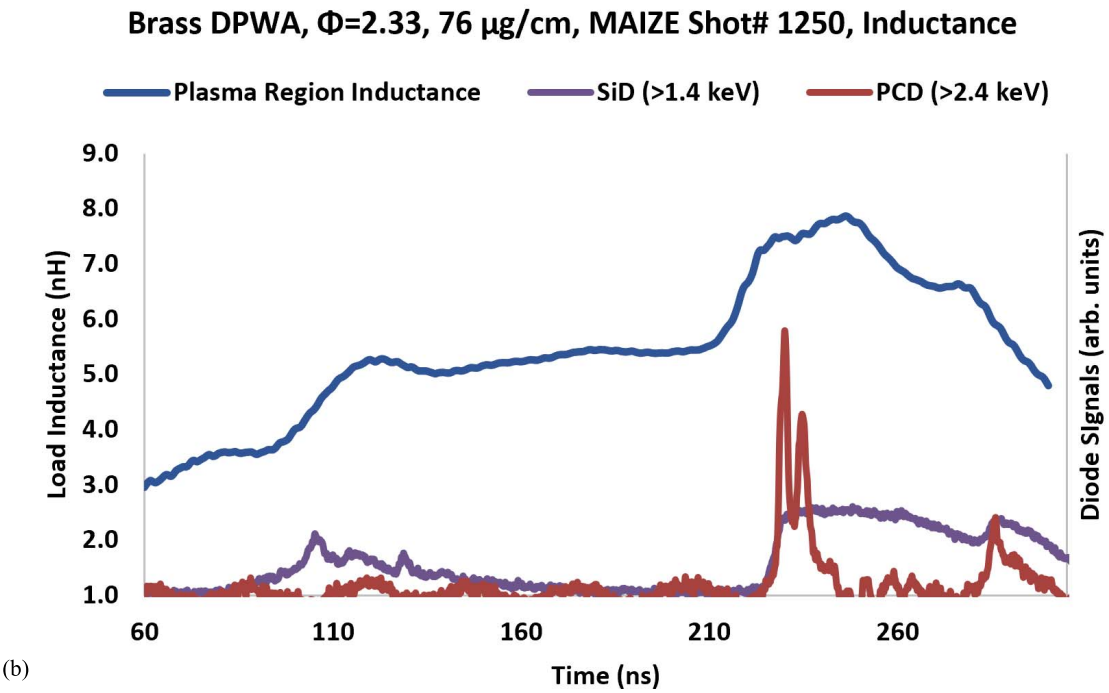

(b)

Fig. 7. (Color online). Inductance calculations from brass DPWA MAIZE Shot 1250. (a) Comparison of simulated current (blue) to the experimentally measured current (orange). (b) Time-dependent load plasma region inductance throughout the implosion (dark blue), plotted with >1.4 keV (purple) and >2.4 keV (dark red) X-ray signals.

(this can be observed in Fig. 3, as the precursor column appears to be "bent" more toward one imploding plane).

VI. Conclusion

To expand upon previous work with low- and high-atomic-number DPWAs on the MAIZE generator, mid-atomic-number brass DPWAs were imploded in order to get a more complete understanding of the radiative properties of metals with varying atomic numbers imploded on the low-impedance MAIZE LTD, in which it was found that the energy radiated in the >2.4 keV band increased with atomic number.

WADM modeling on the brass DPWAs on MAIZE showed a good correlation with shadowgraphy images and radiation bursts, as did previous WADM modeling on brass DPWAs on the Zebra machine. Spectral modeling of the brass DPWAs on MAIZE revealed relatively uniform electron temperatures on the order of 360 eV and a density of 5×10^{19} cm^{-3}, which is cooler than similar loads on the Zebra generator (400–450 eV), but on a similar order of density (10^{19} cm^{-3}) [7]. This cooler plasma temperature on MAIZE is due to the lower maximum current (∼500 kA on MAIZE versus ∼1 MA on Zebra). However, the most intense L-shell Cu and Zn lines were optically thick in experiments on both Zebra and MAIZE.

These results demonstrate many significant findings. The first is that the overall physical processes of DPWA implosions (development of standing shocks, precursor development, radiation burst, and primary implosion) are consistent over a variety of various metals, and across different MA-class drivers of different architectures [7], [14]. Second, the tendencies to radiate from non-LTE L-shell emission as a function of atomic-number are similar between MAIZE and Zebra, from measurements of X-ray energy in several bands. Lastly, an electrical, rather than optical, diagnostic has been developed on MAIZE to estimate the plasma region inductance throughout a wire array pinch, which accurately captures pinch timing, and is somewhat informative on pinch strength (verified by optical diagnostics over a variety of DPWA dimensions and materials), enabling future experiments designed to investigate X-ray emission amplitude and duration to be fielded with minimal and easily realizable diagnostic capabilities. These findings help to show that wire array experiments across both larger and smaller university-scale pulsed power facilities yield similar results, which, in turn, demonstrates that experiments on university-scale machines, like these, could help to inform experimental designs on larger facilities.

ACKNOWLEDGMENT

The authors would like to thank Dr. Ishor K. Shrestha for his help with experiments at the University of Michigan, Ann Arbor, MI, USA. This article describes objective technical results and analysis. Any subjective views or opinions that might be expressed in this article do not necessarily represent the views of the U.S. Department of Energy or the United States Government.

REFERENCES

[1] M. G. Mazarakis *et al.*, "High-current linear transformer driver development at Sandia national laboratories," *IEEE Trans. Plasma Sci.*, vol. 38, no. 4, pp. 704–713, Apr. 2010, doi: 10.1109/TPS.2009.2035318.

[2] W. A. Stygar *et al.*, "Conceptual designs of two petawatt-class pulsed-power accelerators for high-energy-density-physics experiments," *Phys. Rev. Special Topics Accel. Beams*, vol. 18, no. 11, Nov. 2015, doi: 10.1103/PhysRevSTAB.18.110401.

[3] M. E. Cuneo *et al.*, "Magnetically driven implosions for inertial confinement fusion at Sandia national laboratories," *IEEE Trans. Plasma Sci.*, vol. 40, no. 12, pp. 3222–3245, Dec. 2012, doi: 10.1109/TPS.2012.2223488.

[4] R. M. Gilgenbach *et al.*, "MAIZE: A 1 MA LTD-driven Z-pinch at the university of Michigan," in *Proc. AIP Conf. Proc.*, 2009, pp. 259–262, doi: 10.1063/1.3079742.

[5] V. L. Kantsyrev *et al.*, "A review of new wire arrays with open and closed magnetic configurations at the 1.6 MA zebra generator for radiative properties and opacity effects," *High Energy Density Phys.*, vol. 5, no. 3, pp. 115–123, Sep. 2009, doi: 10.1016/j.hedp.2009.04.001.

[6] K. M. Williamson *et al.*, "Implosion dynamics in double planar wire array Z pinches," *Phys. Plasmas*, vol. 17, no. 11, Nov. 2010, Art. no. 112705, doi: 10.1063/1.3511775.

[7] N. D. Ouart *et al.*, "Studies of radiative and implosion characteristics from brass planar wire arrays," *IEEE Trans. Plasma Sci.*, vol. 38, no. 4, pp. 631–638, Apr. 2010, doi: 10.1109/TPS.2010.2040093.

[8] V. L. Kantsyrev *et al.*, "Radiation sources with planar wire arrays and planar foils for inertial confinement fusion and high energy density physics research," *Phys. Plasmas*, vol. 21, no. 3, Mar. 2014, Art. no. 031204, doi: 10.1063/1.4865367.

[9] V. L. Kantsyrev *et al.*, "Compact hohlraum configuration with parallel planar-wire-array X-ray sources at the 1.7-MA Zebra generator," *Phys. Rev. E, Stat. Phys. Plasmas Fluids Relat. Interdiscip. Top.*, vol. 90, no. 6, Dec. 2014, Art. no. 063101, doi: 10.1103/PhysRevE.90.063101.

[10] A. S. Safronova *et al.*, "Larger sized planar wire arrays of complex configuration on 1.5–1.8 MA Z-pinch generator," *Phys. Plasmas*, vol. 23, no. 10, Oct. 2016, Art. no. 101210, doi: 10.1063/1.4965239.

[11] B. Jones *et al.*, "Planar wire-array Z-pinch implosion dynamics and X-ray scaling at multiple-MA drive currents for a compact multisource hohlraum configuration," *Phys. Rev. Lett.*, vol. 104, no. 12, Mar. 2010, Art. no. 125001, doi: 10.1103/PhysRevLett.104.125001.

[12] A. S. Safronova *et al.*, "Double and single planar wire arrays on university-scale low-impedance LTD generator," *IEEE Trans. Plasma Sci.*, vol. 44, no. 4, pp. 432–440, Apr. 2016, doi: 10.1109/TPS.2016.2538291.

[13] V. L. Kantsyrev *et al.*, "Studies of implosion and radiative properties of tungsten planar wire arrays on Michigan's linear transformer driver pulsed-power generator," *IEEE Trans. Plasma Sci.*, vol. 46, no. 11, pp. 3778–3788, Nov. 2018, doi: 10.1109/TPS.2018.2874045.

[14] C. J. Butcher *et al.*, "Load dynamics of double planar foil liners and double planar wire arrays on the UM MAIZE LTD generator," *Phys. Plasmas*, vol. 28, no. 8, Aug. 2021, Art. no. 082702, doi: 10.1063/5.0044058.

[15] A. S. Chuvatin *et al.*, "Operation of a load current multiplier on a nanosecond mega-ampere pulse forming line generator," *Phys. Rev. Special Topics Accel. Beams*, vol. 13, no. 1, Jan. 2010, Art. no. 010401, doi: 10.1103/PhysRevSTAB.13.010401.

[16] M. G. Mazarakis *et al.*, "High current, 0.5-MA, fast, 100-ns, linear transformer driver experiments," *Phys. Rev. Special Topics Accel. Beams*, vol. 12, no. 5, May 2009, Art. no. 050401, doi: 10.1103/PhysRevSTAB.12.050401.

[17] S. Hansen, "Development and application of L-shell spectroscopic modelling for plasma diagnostics," Ph.D. dissertation, Dept. Phys., Univ. Nevada, Reno, Reno, NV, USA, 2003.

[18] A. S. Safronova *et al.*, "Spectroscopic modeling of radiation from Cu and Mo X-pinches produced on the UNR 1 MA zebra generator," *J. Quant. Spectrosc. Radiat. Transf.*, vol. 99, nos. 1–3, pp. 560–571, May 2006, doi: 10.1016/j.jqsrt.2005.05.045.

[19] J. P. Knauer *et al.*, "Response model for Kodak biomax-MS film to X rays," *Rev. Sci. Instrum.*, vol. 77, no. 10, Oct. 2006, Art. no. 10F331, doi: 10.1063/1.2220046.

[20] F. J. Marshall, J. P. Knauer, D. Anderson, and B. L. Schmitt, "Absolute calibration of Kodak biomax-MS film response to X rays in the 1.5-to 8-keV energy range," *Rev. Sci. Instrum.*, vol. 77, no. 10, Oct. 2006, Art. no. 10F308, doi: 10.1063/1.2221698.

[21] M. F. Gu, "The flexible atomic code," *Can. J. Phys.*, vol. 86, no. 5, pp. 675–689, May 2008, doi: 10.1139/P07-197.

[22] D. A. Yager-Elorriaga *et al.*, "Discrete helical modes in imploding and exploding cylindrical, magnetized liners," *Phys. Plasmas*, vol. 23, no. 12, Dec. 2016, Art. no. 124502, doi: 10.1063/1.4969082.

[23] A. M. Steiner *et al.*, "Determination of plasma pinch time and effective current radius of double planar wire array implosions from current measurements on a 1-MA linear transformer driver," *Phys. Plasmas*, vol. 23, no. 10, Oct. 2016, Art. no. 101206, doi: 10.1063/1.4965241.

[24] A. A. Esaulov, A. L. Velikovich, V. L. Kantsyrev, T. A. Mehlhorn, and M. E. Cuneo, "Wire dynamics model of the implosion of nested and planar wire arrays," *Phys. Plasmas*, vol. 13, no. 12, Dec. 2006, Art. no. 120701, doi: 10.1063/1.2402147.

[25] A. A. Esaulov *et al.*, "Wire ablation dynamics model and its application to imploding wire arrays of different geometries," *Phys. Rev. E, Stat. Phys. Plasmas Fluids Relat. Interdiscip. Top.*, vol. 86, no. 4, Oct. 2012, Art. no. 046404, doi: 10.1103/PhysRevE.86.046404.

[26] A. A. Esaulov *et al.*, "WADM and radiation MHD simulations of compact multi-planar and cylindrical wire arrays at 1 MA currents," *High Energy Density Phys.*, vol. 5, no. 3, pp. 166–172, Sep. 2009, doi: 10.1016/j.hedp.2009.03.010.

[27] V. L. Kantsyrev *et al.*, "Anisotropy of radiation emitted from planar wire arrays," *Phys. Plasmas*, vol. 20, no. 7, Jul. 2013, Art. no. 070702, doi: 10.1063/1.4817023.

[28] R. D. McBride *et al.*, "A primer on pulsed power and linear transformer drivers for high energy density physics applications," *IEEE Trans. Plasma Sci.*, vol. 46, no. 11, pp. 3928–3967, Nov. 2018, doi: 10.1109/TPS.2018.2870099.

Christopher J. Butcher was born in San Diego, CA, USA, in 1992. He received the Ph.D. degree in physics from the University of Nevada, Reno (UNR), Reno, NV, USA, in 2022.

He was involved in Z-pinch experiments on the Zebra generator at UNR and the MAIZE LTD generator at the University of Michigan, Ann Arbor, MI, USA. He is currently studying the implosion characteristics of Z-pinches from planar wire arrays and foils.

Victor L. Kantsyrev (Member, IEEE) received the M.S. and Ph.D. degrees from the Moscow Engineering Physics Institute, Moscow, Russia, in 1972 and 1981, respectively, and the Dr.Sc. degree (equivalent to the Dr.Habil. degree in Europe) from the Institute of Analytical Instrumentation Russian Academy of Science, Saint Petersburg, Russia, in 1992.

He was a researcher and the head of sectors and laboratories in several Russian scientific institutes. He joined the Department of Physics, University of Nevada, Reno, NV, USA, in 1994, where he has been a Research Professor since 1996. He was one of the pioneers in research on compact laser- and gas-puff plasmas X-ray sources and the development of X-ray and extreme UV glass capillary optics. His former Ph.D. students are working in National and Federal Laboratories. He has authored or coauthored around 240 scientific papers (including two U.S. patents and five Russian inventor's certificates). His research interests include research on radiative properties and implosion dynamics of planar and cylindrical wire arrays, planar foils, X-pinch, and gas-puff plasmas and their applications for radiation physics and inertial confinement fusion, pulsed power, high-power laser plasmas, the X-ray and EUV plasma diagnostics, surface modification with laser and X-ray beams, X-ray lithography for microelectronics, X-ray microscopy for bio-medicine, and optoelectronics.

Dr. Kantsyrev organized and chaired the technical areas and sessions at the International Conferences on Plasma Science, the Pulsed Power Conference, the International Conference on Dense Z-pinches, and the International Society for Optical Engineers Conferences.

Alla S. Safronova (Member, IEEE) was born in Moscow, Russia. She received the Ph.D. degree in physics from the Institute of General Physics, Russian Academy of Science, Moscow, in 1986.

From 1994 to 1998, she was a Visiting Scientist and then a Post-Doctoral Research Associate with the Department of Physics, University of Nevada, Reno, NV, USA, where she has been an Associate Research Professor since 1998 and is currently a Research Professor. She is one of the pioneers in the application of X-ray line polarization to astrophysical and laboratory plasmas. Her former Ph.D. students are working with Sandia National Laboratories, Albuquerque, NM, USA, the U.S. Naval Research Laboratory, Washington, DC, USA, scientific companies, and also abroad. She has authored or coauthored more than 220 papers. Her current research interests include studying radiation from and processes in high-energy-density plasmas, such as Z-pinch and high-power laser plasmas, and tokamak plasmas.

Dr. Safronova served on the IEEE Plasma Science and Applications Executive Committee from 2015 to 2017. She organized and co-chaired the series of international workshops on radiation from high-energy-density plasmas (RHEDP 2011, 2013, and 2015) and the 10th International Conference on Dense Z-Pinches (DZP2017) and sessions at the International Conferences on Plasma Science (ICOPS) and other international meetings on plasma physics. She was the General Chair of the ICOPS 2021. She was a Guest Editor of the 5th Special Issue of the IEEE TPS on Z-pinch Plasmas in 2012, two special topic sections on RHEDP of Physics of Plasmas in 2014 and 2016, and the 7th Special Issue of the IEEE TPS on Z-Pinch Plasmas in 2018.

Veronica V. Shlyaptseva was born in Moscow, Russia. She received the B.S. degree from the University of Nevada, Reno (UNR), Reno, NV, USA, in 2008.

She was working on X-ray diagnostics and spectroscopy of Z-pinch and laser plasmas and on modeling of hohlraum experiments. She was a Staff Member with UNR. She was involved in Z-pinch experiments on Zebra at UNR and MAIZE at the University of Michigan, Ann Arbor, MI, USA, and in laser-plasma experiments at Leopard laser at UNR and TITAN laser at the Lawrence Livermore National Laboratory, Livermore, CA, USA. She was a key experimentalist in collaboration on Ar, Kr, and Xe gas-puffs with Japan. She is currently with Stratos Consulting, Boston, MA, USA, working on designing database solutions.

Austin Stafford, photograph and biography not available at the time of publication.

Paul C. Campbell, photograph and biography not available at the time of publication.

Stephanie M. Miller, photograph and biography not available at the time of publication.

Nicholas M. Jordan (Senior Member, IEEE) received the B.S.E., M.S.E., and Ph.D. degrees in nuclear engineering and radiological science from the University of Michigan, Ann Arbor, MI, USA, in 2002, 2004, and 2008, respectively.

From 2008 to 2013, he was with Cybernet Systems, Ann Arbor, where he developed technology to disable uncooperative vehicles using microwave pulses. He is currently an Associate Research Scientist with the Plasma, Pulsed Power, and Microwave Laboratory, University of Michigan. His current research interests include pulsed power, laser ablation, Z-pinch physics, plasma discharges, magnetrons, magnetically insulated line oscillators, crossed-field amplifiers, and other high-power microwave devices.

Ryan D. McBride (Member, IEEE) received the Ph.D. degree from Cornell University, Ithaca, NY, USA, in 2009.

He conducted experimental research on wire-array Z-pinch implosions using the 1-MA COBRA pulsed-power facility at Cornell University. From 2008 to 2016, he was with Sandia National Laboratories, Albuquerque, NM, USA, where he held appointments as a Staff Physicist and a Department Manager, where he conducted research in nuclear fusion, radiation generation, and high-pressure material properties using the 25-MA Z pulsed-power facility. He is currently a Professor with the Department of Nuclear Engineering and Radiological Sciences, University of Michigan, Ann Arbor, MI, USA. His research is conducted primarily within the Plasma, Pulsed Power, and Microwave Laboratory, University of Michigan, which includes two linear transformer driver facilities, such as MAIZE (1 MA and 100 ns) and BLUE (150 kA and 100 ns). His research has been focused on both experimental and theoretical studies of magnetized liner inertial fusion (MagLIF). MagLIF is presently one of the USA's three mainline approaches to studying controlled inertial confinement fusion in the laboratory. His current research interests include plasma physics, nuclear fusion, radiation generation, pulsed-power technology, plasma diagnostics, and the dynamics of magnetically driven, cylindrically imploding systems.

Adam M. Steiner (Member, IEEE) received the B.S. degree in nuclear engineering and physics from North Carolina State University, Raleigh, NC, USA, in 2010, and the M.S. and Ph.D. degrees in nuclear engineering and radiological sciences from the University of Michigan, Ann Arbor, MI, USA, in 2012 and 2016, respectively.

From 2016 to 2019, he was with Lockheed Martin Aeronautics, Fort Worth, TX, USA, where he developed megajoule-class pulsed power drivers for plasma sources, neutral beam accelerators, and magnetic confinement coils. He is currently a Pulsed-Power Scientist with Sandia National Laboratories, Albuquerque, NM, USA. His current research interests include mitigating energy loss mechanisms on large pulsed-power facilities and developing improved pulsed-power components, including flashover-resistant composite insulators and sulfur hexafluoride-free spark gap switches.

Ronald M. Gilgenbach (Life Fellow, IEEE) received the B.S. and M.S. degrees received from the University of Wisconsin–Madison, Madison, WI, USA, in 1972 and 1973, respectively, and the Ph.D. degree in electrical engineering from Columbia University, New York, NY, USA, in 1978.

In the early 1970s, he spent several years as a Member of the Technical Staff with Nokia Bell Labs, Holmdel, NJ, USA. From 1978 to 1980, he performed gyrotron research at the U.S. Naval Research Laboratory, Washington, DC, USA, and performed the first electron cyclotron heating experiments on a tokamak plasma in the Oak Ridge National Laboratory, Oak Ridge, TN, USA. He joined the faculty of the University of Michigan (UM), Ann Arbor, MI, USA, in 1980, and founded the Plasma, Pulsed Power and Microwave Laboratory. He is currently the Chihiro Kikuchi Collegiate Professor with the Department of Nuclear Engineering and Radiological Sciences, UM. At UM, he has supervised 50 graduate Ph.D. students.

Dr. Gilgenbach is a fellow of the American Physical Society Division of Plasma Physics and the American Nuclear Society. He received the 1997 IEEE Plasma Science and Applications Committee (PSAC) Award and the 2017 IEEE Peter Haas Pulsed Power Award. He served as the IEEE PSAC Chair from 2007 to 2008. He is a past Associate Editor of the journal *Physics of Plasmas*.